29th Congress of the International Council of the Aeronautical Sciences
St. Petersburg, Russia; September 7-12, 2014

INFLUENCE OF WING ASPECT RATIO ON PASSIVE STALL CONTROL AT LOW REYNOLDS NUMBER USING SINUSOIDAL LEADING EDGES

A. Esmaeili*, J. M. M. Sousa*
***LAETA, IDMEC, Instituto Superior Técnico, Universidade de Lisboa, Lisboa, Portugal**

Keywords: *passive stall control, low Reynolds number, detached eddy simulation*

Abstract

The SST k-ω DDES model has been used to study the influence of wing aspect ratio on passive stall control at low Reynolds number using sinusoidal leading edges. Both stalled and unstalled flow conditions were considered to analyze the effect of low Reynolds number corrections on the performance of the DDES model. It was concluded that major improvements to the foregoing correction are still required to deal with stalled flow conditions and two proposals have been investigated as well.

1 Introduction

Fixed-wing air vehicles operating at low Reynolds numbers are prone to enter aerodynamic stall even when subjected to moderate incidence angles. For instance, in the case of outdoor operation of Micro Air Vehicles (MAV), this frequently results from maneuvering flight or the occurrence of wind gusts. On the other hand, it is known that flow control may be used to delay or smooth out aerodynamic stall with a minimal penalty on performance. The various techniques employed for the foregoing purpose are usually classified as either active or passive. Although a better optimization may, in general, be achieved via the implementation of active flow control, such option involves higher systems complexity and energy consumption by actuators. In a scenario where take-off weight is strongly limited and more space available is desired for the installation of the systems required for the specific mission of the air vehicle, passive flow control emerges as a preferred choice.

A few years ago, a solution to achieve passive stall control via modification of the leading edge to a sinusoidal shape was analyzed in detail for a thick NACA airfoil [1]. The original idea received biomimetic inspiration from observations made to the pectoral flippers of humpback whales [2]. More recently, other studies [3-6] have assessed the outcome of this solution at Reynolds numbers and wing aspect ratios typical of MAV. Although not completely understood due to flow visualization difficulties in the wind tunnel, some of the aforementioned experiments have evidenced the dramatic influence of the aspect ratio on lift characteristics [3]. Namely, it has been shown that, for a unity aspect ratio, wing variants with a sinusoidal leading edge have not been able to generate significant gains with respect the baseline geometry; but the corresponding data for an aspect ratio of 1.5 contrasts strongly with the former as clear benefits have been reported in post-stall conditions from the use of a modified leading edge. It is thought that such a drastic change with only an increase of the wing aspect ratio from 1 to 1.5 is essentially due to a different interaction of the tip vortices with those generated by the scalloped leading edge.

Figure 1 portrays an instantaneous view of the vortical structures generated by the modified leading edge and those produced at the wing tips for unity aspect ratio at a moderate incidence and a low Reynolds number. Eulerian coherent structure detection in the Detached Eddy Simulation (DES) has been achieved by the use of the *Q*-criterion (which locates regions where rotation dominates strain in the flow [7]). The identification of these unsteady structures is

a key issue to understand their interaction. In the case of a unity aspect ratio, the more intense and stable tip vortices seem to be dominant of the wing span, hence preventing the occurrence of stall.

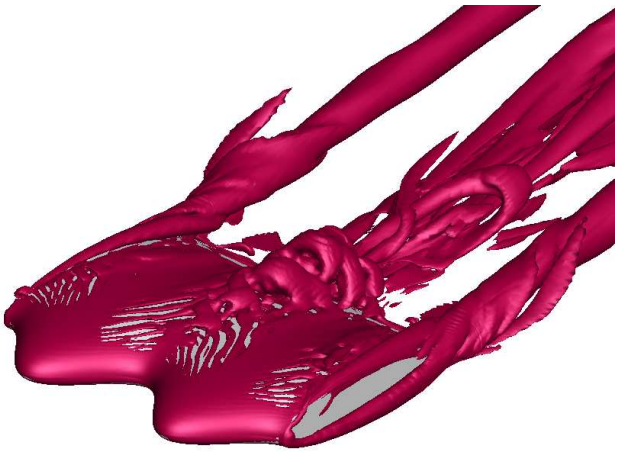

Fig. 1. Instantaneous vortical structures around a unity aspect ratio wing with a modified leading edge at $\alpha = 15^o$ and Re = 140,000.

In the present work, numerical simulations of some of the low-aspect-ratio wings experimentally studied in [3] are carried out with the aim of providing detailed flow information that may allow a better understanding of how the performance of the stall control technique is affected by the change in aspect ratio. Due to the establishment of large regions of separated flow and coexistence of laminar and turbulent flow, DES was deemed as the most appropriate numerical methodology to be employed for this purpose [5]. However, the ability to correctly predict the extent of flow separation and the occurrence of stall at low Reynolds number is essentially limited by the performance of the turbulence modeling [8]. Hence, different approaches will be tested and two procedures for modeling improvement will be also analyzed.

2 Wing Models

The numerical wing models were constructed using a commercial CAD software package, based on a NASA LS(1)-0417 profile (see Fig. 2). In order to generate the sinusoidal leading edge, the reference wing section was modified without distorting the trailing region. The original airfoil was prescribed to the zero amplitude points of the sinus wave. In previous studies [1,3], various values of the amplitude-to-chord ratio A/c and wavelength-to-chord ratio λ/c of the wave (see Fig. 3) have been studied to account for their effect. However, in the present investigation, only A/c = 0.12 and λ/c = 0.5 have been considered, but the values of 1 and 1.5 have been chosen for the variation of the wing aspect ratio AR.

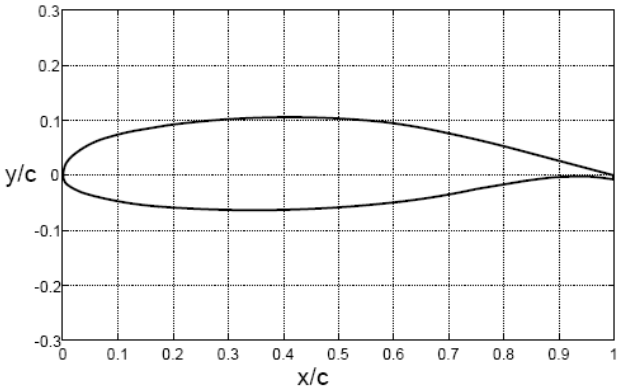

Fig. 2. NASA LS(1)-0417 profile used as baseline section for the wing models.

The profiles located at smaller chord zones than the reference (troughs) exhibit larger leading edge radii and the profiles corresponding to maximum amplitude zones, displaying larger chords (peaks), are relatively thinner than the reference geometry and show a smaller leading edge radius. Naturally, the mean chord of all the models used in the present study was kept constant. In addition, square wing tips have been selected in order to avoid the addition of extra variables to the design of the models.

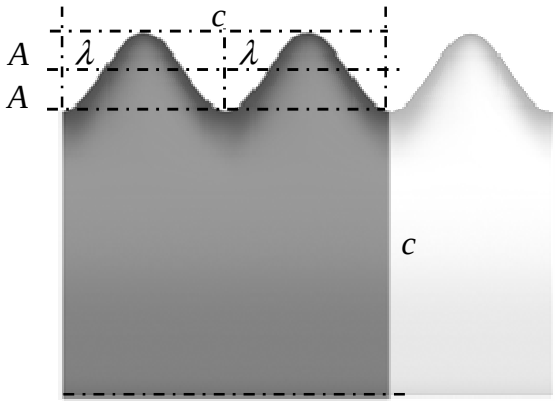

Fig. 3. Geometric definition of the planform of the sinusoidal leading edge wing models.

The computational mesh around the finite wings was generated employing a C-H-topology built with about 10 million and 13 million mesh nodes for the *AR* = 1 and 1.5 wing models, respectively. Farfield boundaries were set at a distance of approximately 20*c*. No-slip conditions were applied along the wall surfaces of the wing. Aiming to properly resolve the wall boundary layers, mesh nodes were clustered near wing surfaces using a geometric expansion. Finally, as the flow remained incompressible in all studied cases, a simple open boundary condition was used at the outflow section.

3 Detached Eddy Simulations

3.1 Basic Formulation

As discussed earlier, DES is known to exhibit a good performance when massive flow separations occur [9], so it was chosen as the fundamental model formulation to be used here in the study of stalled and unstalled regimes. This type of modeling is able to switch explicitly between Reynolds Averaged Navier Stokes (RANS) and Large Eddy Simulation (LES) modes based on the local mesh spacing and turbulent length scale.

However, despite the simplicity of the original DES concept, its use is not straightforward in complex flow application such as the present one [10]. Hence original formulations have been improved to the so-called Delayed Detached Eddy Simulations (DDES), namely to avoid the problems of grid induced separation, with the introduction of shielding functions [10,11]. In addition, it has been argued that the Shear Stress Transport (SST) k-ω turbulence model performs well on reducing the mesh influence of the DES limiter in the RANS boundary layer [9]. This particular turbulence model has been selected for this study taking also into account the foregoing feature.

The governing equations of the SST k-ω DDES model used here are briefly described as follows

$$\frac{\partial \rho k}{\partial t} + \nabla \cdot \left(\rho \vec{U} k\right) = \nabla \cdot \left[(\mu + \sigma_k \mu_t)\nabla k\right] + P_k - \rho\sqrt{k^3}\,/\,l_{DDES} \qquad (1)$$

$$\frac{\partial \rho \omega}{\partial t} + \nabla \cdot \left(\rho \vec{U} \omega\right) = \nabla \cdot \left[(\mu + \sigma_\omega \mu_t)\nabla \omega\right] + \alpha \frac{\rho}{\mu_t} P_k - \beta \rho \omega^2 + 2(1 - F_1)\rho \sigma_{\omega_2} \frac{\nabla k \cdot \nabla \omega}{\omega} \qquad (2)$$

where P_k is the production term of turbulent kinetic energy, and the turbulent viscosity is given by

$$\mu_t = \rho \frac{a_1 k}{\max(a_1 \omega, F_2 S)}. \qquad (3)$$

In Eqs. (1)-(3), F_1 and F_2 are the well-known SST blending functions. Their definition can be found in [10], as well the values for the model constants in the same set of equations.

Variable l_{DDES} in Eq. (1) stands for the DDES length scale, obtained by

$$l_{DDES} = l_{RANS} - f_d \max(0, l_{RANS} - l_{LES}) \qquad (4)$$

where l_{LES} and l_{RANS} are the LES and the RANS length scales, respectively, given by

$$l_{LES} = C_{DES}\,\Delta_{\max}, \qquad l_{RANS} = \frac{\sqrt{k}}{C_\mu \omega}. \qquad (5)$$

The value of the constant C_{DES} in Eq. (5) is also blended here between calibrated k-ε and k-ω values using the blending function F_1, whereas $\Delta_{\max}$ is obtained from the maximum edge length of the local mesh cell. Moreover, the empirical delay function f_d involved in the DDES approach established in Eq. (4) is given by the following expressions:

$$f_d = 1 - \tanh\left[(8 r_d)^3\right], \qquad r_d = \frac{\mu_t + \mu}{\rho \kappa^2 d_w^2 \sqrt{S^2 + \Omega^2}} \qquad (6)$$

where d_w is the distance to the closest wall, κ stands for the von Kármán constant, and S and Ω are the strain rate and vorticity tensor invariants, respectively.

3.2 Low Reynolds Number Corrections

Although the SST k-ω turbulence model has purportedly been developed to take advantage

of the fact that the standard k-ω model was well suited to the simulation of the flow near walls (namely in the viscous sublayer), low Reynolds number corrections (LRC) have still been applied to a variety of cases. The derivation of such corrections has been based on asymptotic consistency [12]. In the context of the k-ω turbulence model, these corrections have been proposed to deal with the occurrence of laminar-to-turbulent transition, formulated with a functional dependency on the turbulent Reynolds number Re_t defined by

$$Re_t = \frac{k}{\nu\,\omega}\,. \tag{7}$$

As explained in detail in [12], additional closure coefficients and constants are introduced in the model governing equations, as follows

$$\alpha^* = \frac{\alpha_0^* + Re_t/R_k}{1 + Re_t/R_k}$$

$$\alpha = \frac{13}{25}\frac{\alpha_0 + Re_t/R_\omega}{1 + Re_t/R_\omega}\frac{1}{\alpha^*} \tag{8}$$

$$\beta^* = \frac{9}{100}\frac{100\,\beta_0/27 + \left(Re_t/R_\beta\right)^4}{1 + \left(Re_t/R_\beta\right)^4}$$

where the three variables in Eq. (8), R_k, R_β and R_ω, control the rate at which the closure coefficients approach their fully turbulent values.

The use of low Reynolds number corrections raises the problem of unwanted activation of these terms in the LES mode for which a remedy has been also proposed [11]. In this case, the LES length scale in Eq. (5) should be replaced by the following relation

$$l_{LES} = \Psi\, C_{DES}\, \Delta_{\max} \tag{9}$$

where Ψ is a function to be sought depending on the specific RANS model employed. The derivation of this function is based upon the subgrid scale form of the model and its comparison to the Smagorinsky model. In order to return to the desired Smagorinsky behavior, the correction function must cancel the tendency obtained [11], so that the asymptotic correction reduces to $\Psi = 1$ when $\mu_t/\mu \to \infty$. Unity is also the value to be applied everywhere if the specific model does not produce a particular tendency, i.e. only a multiplicative constant appears in the obtained Smagorinsky form.

3.3 Results with the Basic Formulation

Initial results have been obtained for two different cases, covering both unstalled and stalled conditions, employing the basic DDES formulation. In addition, one single RANS calculation was also carried out to be used as a reference.

The unstalled flow case was selected from [3], corresponding to AR = 1, α = 15º and a Reynolds number Re = 140,000, which remains unchanged in all cases to be considered in the present investigation. The mean flow field (streamlines and contours of the longitudinal velocity component normalized by the free-stream velocity) obtained with the RANS model is portrayed first in Fig. 4, for the central plane crossing the wing (corresponding to a through in the unity aspect ratio wing; see also Fig. 3).

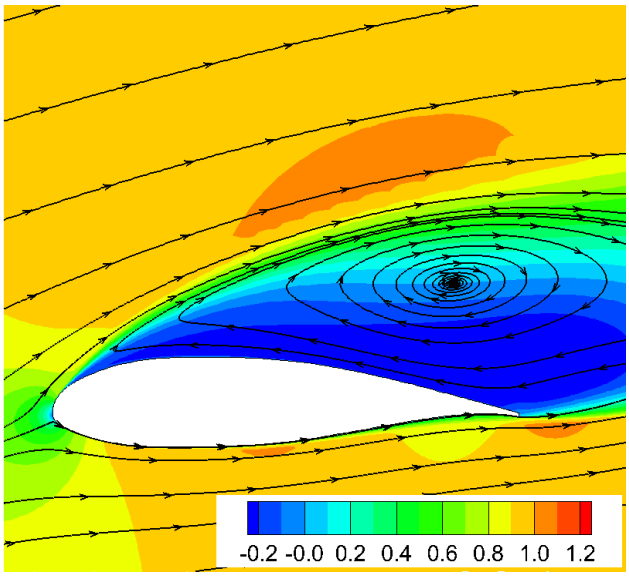

Fig. 4. Mean flow field at a central plane with the RANS model for AR = 1, at α = 15º and Re = 140,000.

A region of massively separated flow is observed in the upper side of the wing for this flow condition, when the SST k-ω RANS model is used. A low Reynolds number correction was not tried in this case because it was expected to increase the extension of flow separation even further. As it might be anticipated, this numerical simulation generated a value of lift coef-

ficient C_L much lower than its experimental counterpart [3] (see Table 1).

Again, based the experimental values of the aerodynamic characteristics, clearly better results have been obtained with the use of the basic DDES formulation (see Table 1). The corresponding results are shown in Fig. 5.

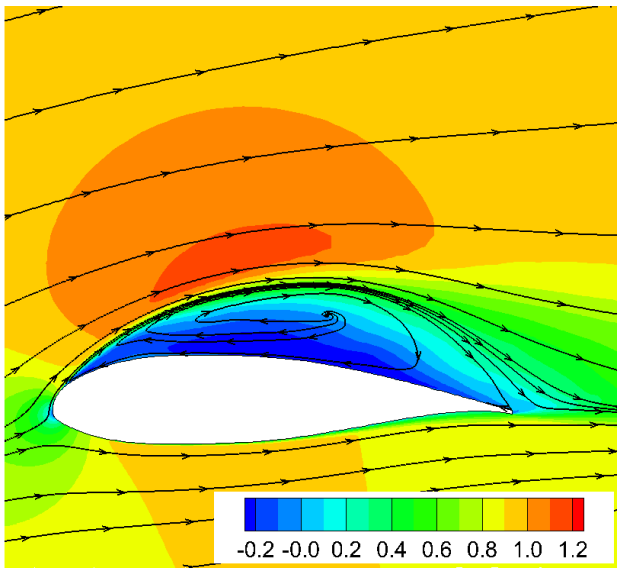

Fig. 5. Mean flow field at a central plane with the basic DDES model for AR = 1, at α = 15º and Re = 140,000.

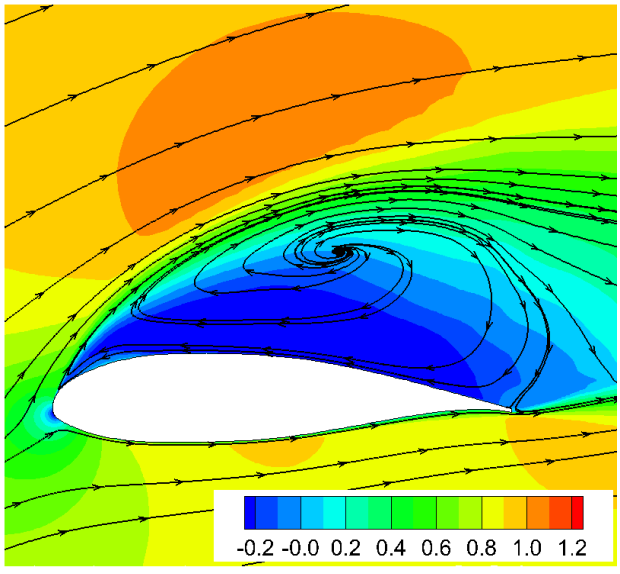

Fig. 6. Mean flow field at a central plane with the basic DDES model for AR = 1.5, at α = 22º and Re = 140,000.

The numerical results obtained for a stalled flow case [3], employing again the basic DDES formulation, now for AR = 1.5, α = 22º, are shown in Fig. 6. These results have been taken at a cross plane corresponding to a through as well (to facilitate the comparison between the two different aspect ratios). However, a smaller extent of flow separation was observed at the central plane for this case (not shown here).

3.4 Results with the Low Reynolds Number Corrections

As an initial step for the study of the results obtained via the use of the DDES model with LRC, the field of turbulent-to-laminar viscosity ratio μ_t/μ is investigated here. However, this analysis has been performed for the flow case with unity aspect ratio only.

Instantaneous fields at a central plane are shown in Figs. 7 and 8, respectively corresponding to the basic DDES model and the DDES model with LRC. The results with the LRC portray a much larger region in the vicinity of the walls exhibiting laminar values of viscosity. This observation seems to be consistent with the physical scenario expected for the studied Reynolds number, which ultimately may explain the better performance of the LRC model concerning drag coefficient C_D, although the difference in C_L with respect to the basic model is within error bands of the experimental data with wind tunnel corrections [3] (see table 1).

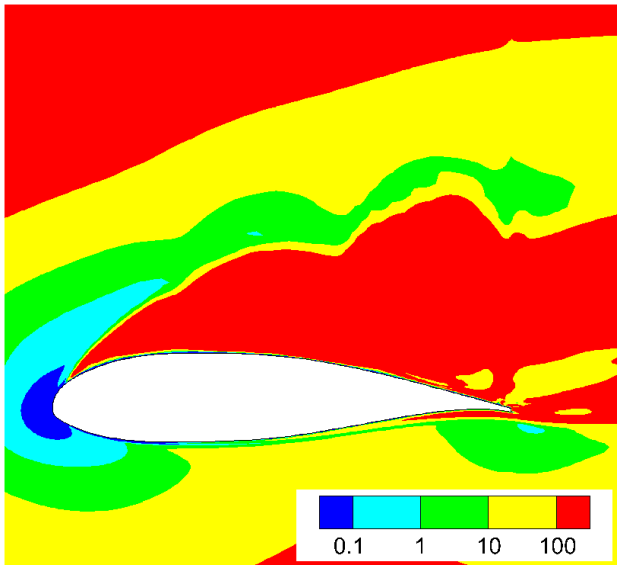

Fig. 7. Instantaneous field of turbulent-to-laminar viscosity ratio at a central plane for the basic DDES model (AR = 1).

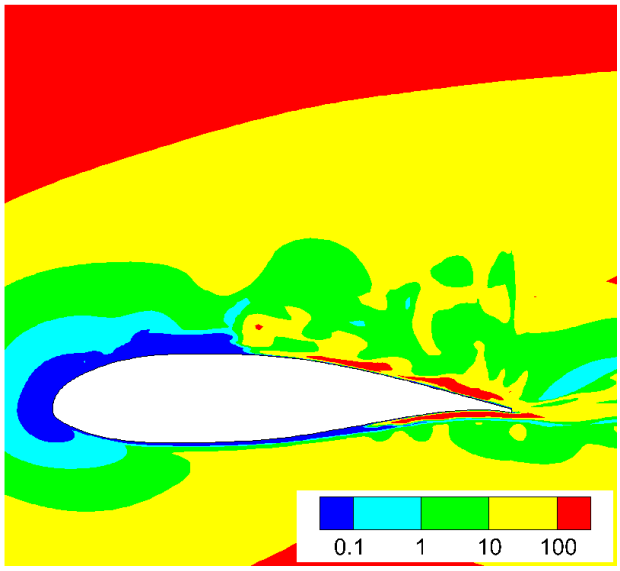

Fig. 8. Instantaneous field of turbulent-to-laminar viscosity ratio at a central plane for the DDES model with LRC (AR = 1).

Table 1. Unstalled flow case data (AR = 1).

Model	C_L	C_D
RANS	0.441	0.154
Basic DDES	0.623	0.180
DDES with LRC	0.644	0.154
Experiments [3]	0.62	0.13

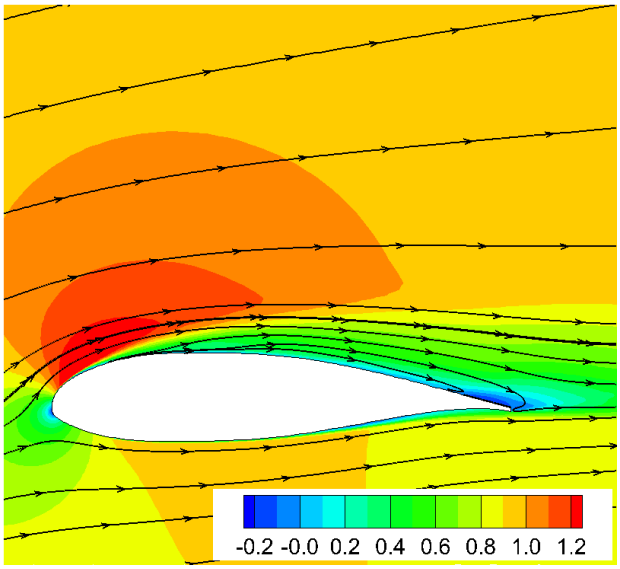

Fig. 9. Mean flow field at a central plane with the DDES model with LRC for AR = 1, at $\alpha = 15^o$ and Re = 140,000.

Numerical simulations to obtain the mean flow fields produced by the DDES model with LRC have therefore been carried out, for both unstalled and stalled flow cases. The foregoing results are shown in Figs. 9 and 10, and should be directly compared with those depicted in Figs. 5 and 6, respectively.

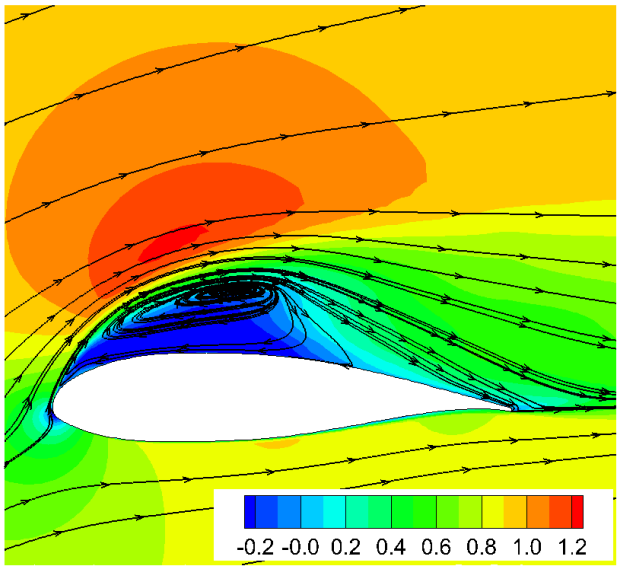

Fig. 10. Mean flow field at a central plane with the DDES model with LRC for AR = 1.5, at $\alpha = 22^o$ and Re = 140,000.

The numerical results obtained for the case of *AR* = 1 demonstrate indeed that, globally, the DDES model with LRC has been able to deal with the unstalled flow conditions satisfactorily. However, slight improvements should still be sought, as will be discussed in the next sub-section. Unfortunately, a similar performance could not be attained for the case of *AR* = 1.5, corresponding to a stalled flow condition. The foreseen drop in C_L was not obtained with the use of LRC, resulting in values even larger than those generated by the basic DDES model. In this case, both models have shown rather poor results, significantly overpredicting both aerodynamic characteristics (see Table 2). Hence, major improvements must definitely be introduced to the SST k-ω DDES model to deal with stalled conditions at this low Reynolds number.

Table 2. Stalled flow case data (AR = 1.5).

Model	C_L	C_D
Basic DDES	0.906	0.354
DDES with LRC	1.020	0.350
Experiment [3]	0.72	0.27

3.5 Improvements to the DDES Model with Low Reynolds Number Corrections

Aiming to improve the performance of the DDES model with low Reynolds number corrections, the Ψ function in Eq. (9) has been derived for the SST k-ω turbulence model. Following the requisites previously indicated in subsection 3.3, the expression reads as

$$\Psi = \left\{ \frac{\beta_1 \alpha \omega \left[\max\left(\frac{1}{\alpha^*}, \frac{F_2 S}{a_1 \omega} \right) \right]^2}{\alpha_1 \beta \omega_\infty} \right\}^{3/4} \qquad (10)$$

where the various coefficients are model constants [13], α^* is given in Eq. (8) and ω_∞ denotes the freestream value of ω.

For the sake of brevity, only the results for the flow case with AR = 1 are shown here. The effect of the function Ψ on the DES length scale of the DDES model with LRC may be appreciated by comparing the instantaneous flow fields at a central plane shown in Figs. 11 and 12, respectively with $\Psi = 1$ (no additional correction) and with the use of Eq. (10). It can be seen that, with the use of Ψ, the strong mesh dependency of the DES length scale has been significantly reduced and a more consistent behavior towards LES regions is also obtained.

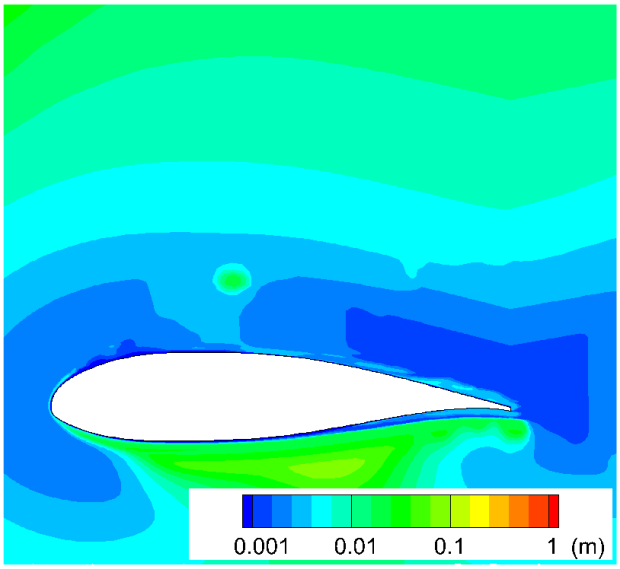

Fig. 11. Instantaneous field of DES length scale at a central plane with Ψ = 1 (AR = 1).

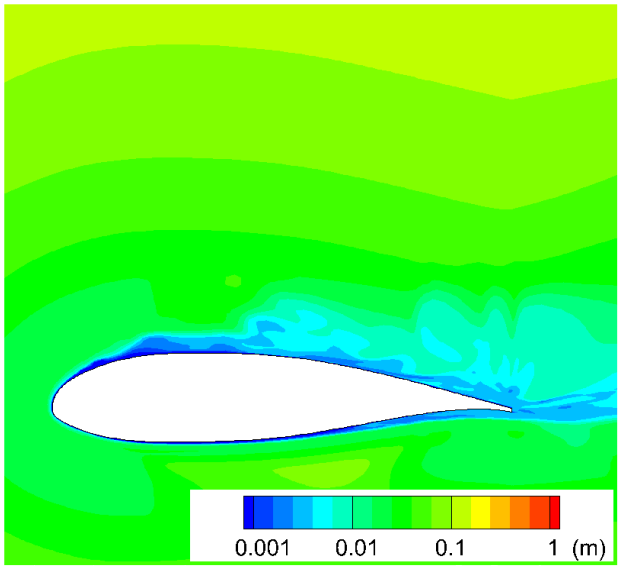

Fig. 12. Instantaneous field of DES length scale at a central plane with function Ψ (AR = 1).

Although the preliminary results of the study of the effect of the function Ψ in Eq. (9) have shown already to be promising, the three coefficients controlling the rate of decay of the LRC in Eq. (8) have also been studied for the SST k-ω turbulence model. As suggested in [12], perturbation methods have been employed to analyze the viscous sublayer. It is aimed that more suitable values of R_k, R_β and R_ω to be used together with the present turbulence model may be obtained, ultimately allowing additional improvements to the low Reynolds number correction procedures previously outlined.

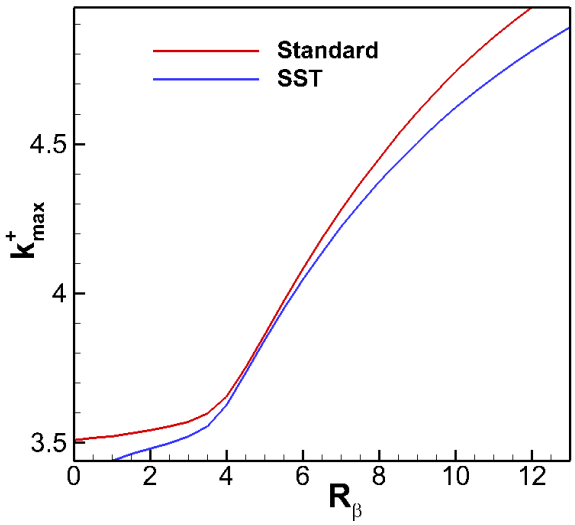

Fig. 13. Variation of the peak value of k^+ with R_β when $R_k = 6$ for standard and SST models.

The relation between coefficient R_β and the peak value of k in wall units k^+_{max}, obtained for the constant in the law of the wall $C = 5.1$ given by the SST model without viscous modifications and assuming $R_k = 6$, is shown in Fig. 13. The results obtained for the standard version of model [12], corresponding to $C = 5.5$, have also been included in the whole analysis, to be used as a reference. It can readily be seen that, as a rule, the SST model is associated to higher values of k^+_{max} for the same value of R_β, when compared to the standard version.

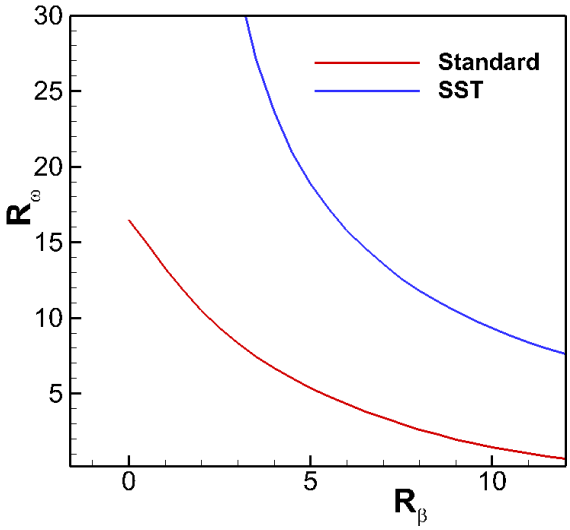

Fig. 14. Variation of R_ω with R_β when $R_k = 6$ for standard and SST models.

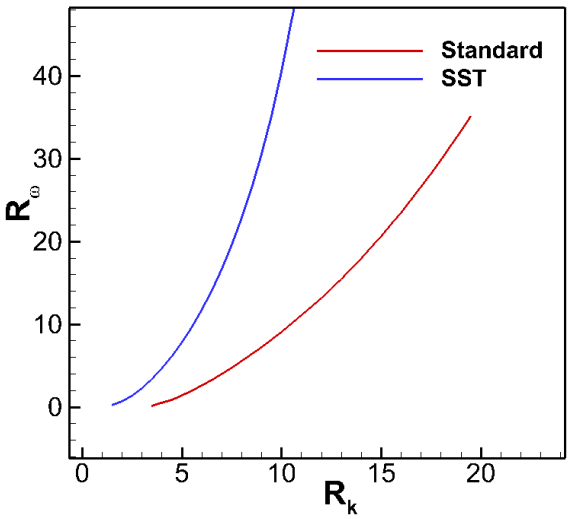

Fig. 15. Variation of R_ω with R_k when $R_\beta = 8$ for standard and SST models.

However, the most striking differences in the studied dependencies for the two versions of the turbulence model are depicted in Figs. 14 and 15. Clearly, these results indicate that the values used in Eq. (8) of the LRC, corresponding to the standard model (namely $R_k = 6$ and $R_\beta = 8$) are not the most suited ones to be employed when the SST version has been selected. However, numerical experiments using SST k-ω DDES model with accordingly modified LRC are still required to achieve a final conclusions on this matter.

4 Conclusions

The capabilities of the SST k-ω DDES model for the numerical simulation of the influence of the wing aspect ratio on passive stall control at low Reynolds number using sinusoidal leading edges have been assessed. Two flow conditions, portraying both stalled and unstalled regimes have been considered. Low Reynolds number corrections to the DDES model have been included. The latter modeling has shown to perform satisfactorily for the unstalled flow condition, whereas drastic improvements are required for the stalled flow condition. This goal has been analyzed employing the subgrid scale form of the model and also perturbation methods for the sublayer region.

Acknowledgement

This work was funded by the Portuguese Government through “Fundação para a Ciência e a Tecnologia”, in the scope of project NATURE (PTDC/EME-MFE/122849/2010).

References

[1] Johari H, Henoch C, Custodio D and Levshin A. Effects of leading-edge protuberances on airfoil performance. *AIAA Journal*, Vol. 45, No. 11, pp 2634-2641, 2007.

[2] Fish F E and Battle J M. Hydrodynamic design of the humpback whale flipper. *Journal of Morphology*, Vol. 225, No. 1, pp 51-60, 1995.

[3] Guerreiro J L E and Sousa J M M. Low-Reynolds-number effects in passive stall control using

Sinusoidal leading edges. *AIAA Journal*, Vol. 50, No. 2, pp 461-469, 2012.

[4] Dropkin A, Custodio D, Henoch C W and Johari H. Computation of flowfield around an airfoil with leading-edge protuberances. *Journal of Aircraft*, Vol. 49, No. 5, pp 1345-1355, 2012.

[5] Câmara J F D and Sousa J M M. Numerical study on the use of a sinusoidal leading edge for passive stall control at low Reynolds number. *Proc 51st AIAA Aerospace Sciences Meeting*, AIAA Paper 2013-0062, 2013.

[6] Zhang M M, Wang G F and Xu J Z. Aerodynamic control of low-Reynolds-lumber airfoil with leading-edge protuberances. *AIAA Journal*, Vol. 51, No. 8, pp 1961-1971, 2013.

[7] Hunt J C R, Wray A A and Moin P. Eddies, stream, and convergence zones in turbulent flows. Center for Turbulence Research, Rep. CTR-S88, 1988.

[8] Delgado H E C, Esmaeili A and Sousa J M M. Stereo PIV o low-aspect-ratio low-Reynolds-number wings with sinusoidal leading edges for improved computational modeling. *Proc 52nd AIAA Aerospace Sciences Meeting*, AIAA Paper 2014-0062, 2014.

[9] Bunge U, Mockett C and Thiele F. Guidelines for implementing detached-eddy simulation using different models. *Aerospace Science and Technology*, Vol. 11, No. 5, pp 376-385, 2007.

[10] Menter F R, Kuntz M and Langtry R. Ten years of experience with the SST turbulence model. *Proc 4th International Symposium on Turbulence and Mass Transfer*, pp 625-632, 2003.

[11] Spalart P R, Deck S, Shur M L, Squires K D, Strelets M K and Travin A. A new version of detached-eddy simulation, resistant to ambiguous grid densities. *Theoretical and Computational Fluid Dynamics*, Vol. 20, pp 181-195, 2006.

[12] Wilcox D C. *Turbulence modeling for CFD*. 3rd edition, DCW Industries, Inc., 2006.

[13] Gritskevitch M S, Garbaruk A V, Schütze J and Menter F R. Development of DDES and IDDES for the k-ω shear stress transport model. *Flow, Turbulence and Combustion*, Vol. 88, pp 431-449, 2012.

Copyright Statement

The authors confirm that they, and/or their company or organization, hold copyright on all of the original material included in this paper. The authors also confirm that they have obtained permission, from the copyright holder of any third party material included in this paper, to publish it as part of their paper. The authors confirm that they give permission, or have obtained permission from the copyright holder of this paper, for the publication and distribution of this paper as part of the ICAS 2014 proceedings or as individual off-prints from the proceedings.